Tunable nonlinear absorption of hydrogenated nanocrystalline silicon

Y. J. Ma,[1] J. I. Oh,[1,2] D. Q. Zheng,[1] W. A. Su,[1] and W. Z. Shen[1,*]

[1]*Laboratory of Condensed Matter Spectroscopy and Opto-Electronic Physics, and Key Laboratory of Artificial Structures and Quantum Control (Ministry of Education), Department of Physics, and Institute of Solar Energy, Shanghai Jiao Tong University, 800 Dong Chuan Road, Shanghai 200240, China*

[2]*Department of Physics, Boston College, Chestnut Hill, Massachusetts 02467, USA*

**Corresponding author: wzshen@sjtu.edu.cn*

Received July 5, 2011; revised August 7, 2011; accepted August 7, 2011; posted August 9, 2011 (Doc. ID 150386); published August 29, 2011

Nonlinear absorption (NLA) of hydrogenated nanocrystalline silicon (nc-Si:H) has been investigated through the open aperture *Z*-scan method for the photon energy of the incident irradiance slightly less than the bandgap of the sample. NLA responses have been observed to be highly sensitive to the wavelength and intensity of the incident irradiance as well as to the bandgap of the sample, indicating greatly tunable NLA of nc-Si:H. The band tail of nc-Si:H appears to play a crucial role in such NLA responses.

OCIS codes: 160.4236, 190.0190, 230.1150, 250.5590, 320.7130.

Hydrogenated nanocrystalline silicon (nc-Si:H), silicon nanocrystals (Si-ncs) embedded in a disordered amorphous Si:H (a-Si:H) matrix, has great potential in optoelectronic applications [1–6]. Since it can be grown by plasma-enhanced chemical vapor deposition (PECVD), nc-Si:H is readily able to be integrated with most Si-based devices [7,8]. Although there have been a great number of studies of nc-Si:H, including linear optical [9], electrical [10], and quantum confinement [11] properties, nonlinear optical properties, especially critical to photonic applications such as all-optical switching [8,12], have not been much investigated to date.

Here, we show greatly tunable nonlinear absorption (NLA) responses of nc-Si:H thin films with the incident irradiance and the bandgap, observed by open aperture (OA) *Z*-scan measurements [13] with the photon energy of the incident irradiance slightly less than their bandgaps. We also show these NLA responses can be well-described by the modified third-order NLA differential equation [14,15]. In addition, we propose that band tail states may be responsible for the NLA behavior of nc-Si:H.

nc-Si:H thin films were grown on glass substrates by PECVD at a radiofrequency (rf) of 13.56 MHz, a total gas ($SiH_4 + H_2$) flow rate of 150 sccm, a chamber pressure of 150 Pa, and a temperature of 250 °C. The silane content was kept constant at ~1% while the rf power density was controlled between 0.17 and 0.61 W/cm^2 to achieve different grain sizes corresponding to different bandgaps. Figure 1(a) shows an X-ray diffraction (XRD) pattern of one of the samples measured by Bruker D8 Discover X-ray diffractometer. From this XRD pattern, the mean crystalline grain size was calculated to be 6.0 nm by using the Scherrer formula. It was also confirmed by a high-resolution transmission electron microscopy (HR-TEM, CM200, Philips), as shown in the inset in Fig. 1(a). Although the data are not shown here, we found the crystalline volume fraction of ~37% from micro-Raman spectroscopy measurements.

We employed *n* & *k* Analyzer 1280 spectrophotometer to measure the wavelength-dependent transmission spectrum ($\lambda = 200$–1000 nm, not shown) from which we extracted the film thickness L (=1.65 μm) and the optical constants including the linear refractive index n and extinction coefficient k. The λ-dependent k is shown in Fig. 1(b), which is an important parameter to calculate the transmittance in Eq. (2). Also, as shown in the inset in Fig. 1(b), we exploited a Tauc plot, i.e., $(\alpha_0 h\nu)^{1/\gamma}$ versus the photon energy $h\nu$ for $\gamma = 2$ (indirect transition) [9,16] to determine the optical bandgap E_g, where the linear absorption coefficient $\alpha_0 = 4\pi k/\lambda$. This Tauc plot shows the linearity at the absorption edge, yielding $E_g = 1.63$ eV.

For the OA *Z*-scan technique, we used a mode-locked Ti:sapphire laser (Spectra-Physics 3960d-X3S), generating nearly Gaussian shape TEM_{00} laser pulses of ~100 fs duration, 82 MHz repetition rate, and tunable wavelength ($\lambda = 775$–800 nm). The transmitted pulses are focused at the sample space through a lens of 75 mm focal length. The beam waist is ~25.5 μm. A lock-in amplifier (PerkinElmer 7265) was also used to regulate both the light chopper (1 kHz) and the signal detector (New Focus 2031) for high signal-to-noise ratio.

We present in Figs. 2(a)–2(d) λ-dependent *Z*-scan transmission (T) spectra of the sample of $E_g = 1.63$ eV at a fixed incident irradiance $I_0 = 2.39$ GW/cm^2. Here, I_0 is the intensity of laser pulses at focus excluding Fresnel reflection loss [13]. As in the figures, this NLA behavior appears to be highly sensitive to λ. At a long $\lambda = 800$ nm in Fig. 2(a), the absorption decreases

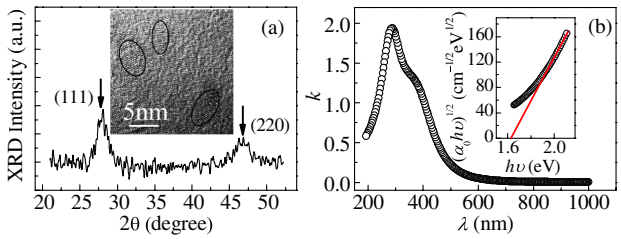

Fig. 1. (Color online) (a) XRD spectrum. Inset is a high-resolution transmission electron microscope image, showing the crystalline grain size indicated with ovals. (b) Extinction coefficient spectrum. Inset is a Tauc plot, where the linear extrapolation (red) is also shown.

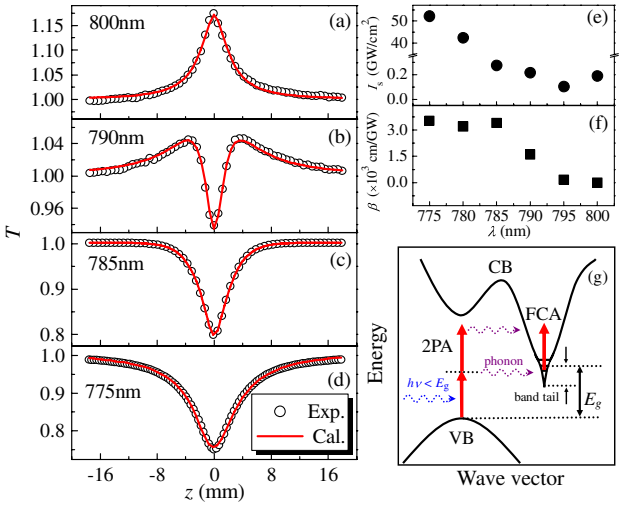

Fig. 2. (Color online) (a)–(d) Measured and calculated Z-scan curves for various wavelengths at a fixed irradiance, $I_0 = 2.39\,\mathrm{GW/cm^2}$. (e), (f) λ-dependent I_s and β. (g) Schematic bandgap diagram showing feasible NLA mechanisms.

(i.e., T increases) as the irradiance increases (i.e., $|z|$ decreases), showing saturable absorption (SA). With a small amount of decreased λ to 775 nm, this nonlinear SA rapidly evolves into reverse SA (RSA) in Fig. 2(d) via the intermediate NLA responses in Figs. 2(b) and 2(c). Note that we also carried out Z-scan measurements on the glass substrate and found no such NLA behavior. This SA-to-RSA switching driven by λ is our new observation in silicon materials, although it has been reported in some other materials, such as azobenzene [17], bisphthalocyanine [18], and GaN [19]. As is shown in Fig. 3(a), the SA-to-RSA switching can be driven also by I_0 as observed in Si-ncs suspended in glycerol [20], Pt nanoparticles [14], and gold nanoparticle array [21].

The observed NLA behavior can be understood in terms of the modified third-order NLA differential equation as in [14,15]:

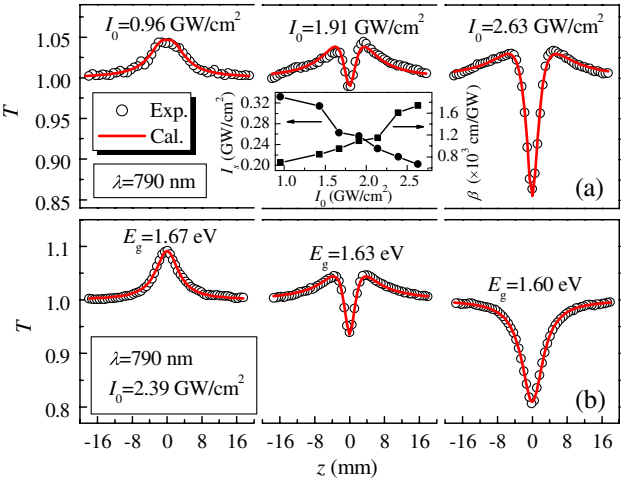

Fig. 3. (Color online) (a) Z-scan curves for various irradiances at a fixed wavelength. Inset shows I_0-dependent I_s and β. (b) Z-scan curves for different bandgaps at fixed wavelength and irradiance.

$$\frac{dI}{dz'} = \alpha(I)I = \left(\frac{\alpha_0}{1 + I/I_s} + \beta I\right)I, \tag{1}$$

where I is the beam irradiance, z' the propagation distance within the sample, and $\alpha(I)$ is the total absorption coefficient. The latter consists of two NLA components, i.e., the SA term $\alpha_0/(1 + I/I_s)$ and the RSA term βI. α_0 is the linear absorption coefficient mentioned earlier, I_s the saturation irradiance characterizing SA, and β the effective NLA coefficient characterizing RSA. Note that, if $I_s \gg I$, the SA term approaches α_0, implying that the larger the I_s, the weaker the SA. The transmittance at the sample position z for OA Z-scan can be expressed as

$$T(z) = \frac{\int_{-\infty}^{+\infty} \mathrm{d}t \int_0^{+\infty} I_{\mathrm{out}} r \mathrm{d}r}{\exp(-\alpha_0 L) \int_{-\infty}^{+\infty} \mathrm{d}t \int_0^{+\infty} I_{in} r \mathrm{d}r}, \tag{2}$$

where I_{in} is the Gaussian shape input irradiance as in [15] and I_{out} the output irradiance that can be expressed in an infinite polynomial series from solving Eq. (1) by using the Adomian decomposition method (ADM) [15]. As clearly seen in Figs. 2(a)–2(d), the calculated transmittance (red solid curves) excellently fits the experimental Z-scan results (black open circles). Note that the first five terms of the Adomian polynomials were taken into account for the fitting process. The λ-dependent nonlinear coefficients I_s and β are presented in Figs. 2(e) and 2(f), resulting from the best fits. At $\lambda = 800$ nm, I_s is $0.19\,\mathrm{GW/cm^2}$ and β is nearly 0, indicating a nearly pure SA. As λ decreases, both I_s and β overall increase, implying that SA becomes weakened while RSA does enhanced. Finally, at $\lambda = 775$ nm, I_s is $52\,\mathrm{GW/cm^2}$ ($\gg I_0 = 2.39\,\mathrm{GW/cm^2}$) and β is 3.5×10^3 cm/GW, indicating a nearly pure RSA.

Now, we want to discuss the physical origin of the NLA behavior in Fig. 2. In our measurements, the photon energy of the incident irradiance varied from 1.55 to 1.60 eV (i.e., λ from 800 to 775 nm), slightly less than the bandgap ($E_g = 1.63$ eV) of the sample. Since nc-Si:H is known to have the exponential band tail of the width ~60 meV [22,23], excited electrons upon the below-bandgap incident irradiance may transit from the valence band to the conduction band tail through a phonon-assisted one-photon absorption (1PA) process as depicted in Fig. 2(g), leading to the absorption saturation of band tail states, i.e., SA, as in Fig. 2(a). As the photon energy of the incident irradiance becomes closer to the bandgap (i.e., for a shorter λ) at a given I_0, it is more difficult to reach an absorption saturation since the number of band tail states increases with increasing energy. As a result, the SA effect should abate with decreasing λ, as in Figs. 2(b)–2(d). This abating behavior of SA is reflected in Fig. 2(e). At the same time, the RSA effect is apparently more distinct as the photon energy of the incident irradiance becomes closer to the bandgap, as in Fig. 2(f). Two kinds of two-photon absorption (2PA) processes may be responsible for RSA: phonon-assisted 2PA via a virtual intermediate state and 1PA-induced free carrier absorption (FCA). The latter process appears to induce the observed RSA, since more electrons are allowed to

exist in the conduction band tail for the larger photon energy of the incident irradiance, likely resulting in a higher chance of FCA. The former process, however, may be responsible for RSA in the case of the far-below-bandgap incident irradiance as observed in GaN [19]. Considering these two feasible processes, β can be written as [24]

$$\beta = \beta_0 + \sigma_{\mathrm{FC}}\alpha_0\tau_0/h\nu, \tag{3}$$

where β_0 is the 2PA coefficient characterizing the former process, σ_{FC} is the FCA cross section, and τ_0 the laser pulse duration. Since β_0 can be neglected in our RSA case, σ_{FC} is proportional to β and one can estimate that $\sigma_{\mathrm{FC}} \sim 6.8 \times 10^{-15}\,\mathrm{cm}^2$ at 775 nm.

We have also performed Z-scan measurements on the sample of $E_g = 1.63$ eV for different incident irradiances. Figure 3(a) shows I_0-dependent Z-scan transmission spectra (black open circles) at a fixed $\lambda = 790$ nm (i.e., 1.57 eV), which are apparently well-described by Eq. (2) (red solid curves). For a low irradiance $I_0 = 0.96\,\mathrm{GW/cm}^2$, although SA and RSA both appear to be weak since I_s is big and β is small, as shown in the inset of Fig. 3(a), SA appears to dominate the NLA. As I_0 increases, I_s decreases but β increases, implying that SA and RSA both become stronger. However, RSA clearly dominates the NLA with increasing I_0.

Finally, in Fig. 3(b), we show the bandgap E_g dependence of the NLA. As seen, these E_g-dependent NLA responses are again well-described by Eq. (2). By tuning E_g from 1.67 to 1.60 eV at fixed λ ($hc/\lambda < E_g$) and I_0, we again observe the SA-to-RSA switching via an intermediate NLA state. This E_g-driven switching is essentially of the same origin as the λ-driven one in Fig. 2, since a decrease of E_g at a fixed λ is effectively the same as an decrease of λ at a fixed E_g. Nonetheless, the E_g-driven switching demonstrates nc-Si:H to be an excellent candidate for NLA applications, since its bandgap can be easily tuned during the growing process.

In summary, we have used the OA Z-scan technique to observe NLA responses of nc-Si:H greatly tunable with the incident irradiance (its wavelength and intensity) and the bandgap of the sample. These NLA responses have turned out to be well-described by the modified third-order NLA equation, suggesting that the NLA mechanism of nc-Si:H may rely on its band tail states. These greatly tunable NLA responses can be utilized for developing highly sensitive photonic devices.

The authors would like to thank T. C. Zhang at National Sun Yat-Sen University for the n & k test and Gu Bing at Nankai University for the helpful discussions in ADM. This work was supported by the National Major Basic Research Project of 2010CB933702 and the National Natural Science Foundation of China (NSFC) under contracts 10734020 and 11074169.

References

1. G. Conibeer, M. Green, R. Corkish, Y. Cho, E. C. Cho, C. W. Jiang, T. Fangsuwannarak, E. Pink, Y. Huang, and T. Puzzer, Thin Solid Films **511**, 654 (2006).
2. S. Tiwari, F. Rana, H. Hanafi, A. Hartstein, E. F. Crabbe, and K. Chan, Appl. Phys. Lett. **68**, 1377 (1996).
3. Y. Tan, T. Kamiya, Z. Durrani, and H. Ahmed, J. Appl. Phys. **94**, 633 (2003).
4. Z. Z. Yuan, A. Anopchenko, N. Daldosso, R. Guider, D. Navarro-Urrios, A. Pitanti, R. Spano, and L. Pavesi, Proc. IEEE **97**, 1250 (2009).
5. S. Sriraman, S. Agarwal, E. S. Aydil, and D. Maroudas, Nature **418**, 62 (2002).
6. B. Jalali and S. Fathpour, J. Lightwave Technol. **24**, 4600 (2006).
7. K. Narayanan and S. F. Preble, Opt. Express **18**, 8998 (2010).
8. A. Martinez, J. Blasco, P. Sanchis, J. V. Galan, J. Garcia-Ruperez, E. Jordana, P. Gautier, Y. Lebour, S. Hernandez, R. Spano, R. Guider, N. Daldosso, B. Garrido, J. M. Fedeli, L. Pavesi, and J. Marti, Nano Lett. **10**, 1506 (2010).
9. H. Chen, M. Gullanar, and W. Z. Shen, J. Cryst. Growth **260**, 91 (2004).
10. X. Y. Chen, W. Z. Shen, H. Chen, R. Zhang, and Y. L. He, Nanotechnology **17**, 595 (2006).
11. L. Bagolini, A. Mattoni, G. Fugallo, L. Colombo, E. Poliani, S. Sanguinetti, and E. Grilli, Phys. Rev. Lett. **104**, 176803 (2010).
12. F. Z. Henari, K. Morgenstern, W. J. Blau, V. A. Karavanskii, and V. S. Dneprovskii, Appl. Phys. Lett. **67**, 323 (1995).
13. M. Sheik-Bahae, A. Said, T. Wei, D. Hagan, and E. Van Stryland, IEEE J. Quantum Electron. **26**, 760 (1990).
14. Y. Gao, X. Zhang, Y. Li, H. Liu, Y. Wang, Q. Chang, W. Jiao, and Y. Song, Opt. Commun. **251**, 429 (2005).
15. J. Wang, B. Gu, H. T. Wang, and X. W. Ni, Opt. Commun. **283**, 3525 (2010).
16. E. D. Palik, ed., *Handbook of Optical Constants of Solids* (Academic, 1985).
17. R. Rangel-Rojo, S. Yamada, H. Matsuda, and D. Yankelevich, Appl. Phys. Lett. **72**, 1021 (1998).
18. K. Unnikrishnan, J. Thomas, V. Nampoori, and C. Vallabhan, Appl. Phys. B **75**, 871 (2002).
19. Y. L. Huang, C. K. Sun, J. C. Liang, S. Keller, M. P. Mack, U. K. Mishra, and S. P. DenBaars, Appl. Phys. Lett. **75**, 3524 (1999).
20. S. Korovin, A. Orlov, A. Prokhorov, V. Pustovoi, M. Konstantaki, S. Couris, and E. Koudoumas, Quantum Electron. **31**, 817 (2001).
21. K. Wang, H. Long, M. Fu, G. Yang, and P. Lu, Opt. Lett. **35**, 1560 (2010).
22. L. Chen, J. Tauc, and Z. Vardeny, Phys. Rev. B **39**, 5121 (1989).
23. A. F. Halverson, J. J. Gutierrez, J. D. Cohen, B. Yan, J. Yang, and S. Guha, Appl. Phys. Lett. **88**, 071920 (2006).
24. N. Kamaraju, S. Kumar, A. Sood, S. Guha, S. Krishnamurthy, and C. Rao, Appl. Phys. Lett. **91**, 251103 (2007).